Sensors and Actuators B 266 (2018) 793–804

Contents lists available at ScienceDirect

Sensors and Actuators B: Chemical

journal homepage: www.elsevier.com/locate/snb

Mixed-potential-type NO_2 sensors based on stabilized zirconia and CeO_2-B_2O_3 (B = Fe, Cr) binary nanocomposites sensing electrodes

Rui You [a], Tianshuang Wang [b], Hongyan Yu [a], Jing Wang [b], Geyu Lu [b], Fangmeng Liu [b,*], Tianhong Cui [c,*]

[a] Department of Precision Instrument, Tsinghua University, Beijing, 100084, China
[b] State Key Laboratory on Integrated Optoelectronics, College of Electronic Science and Engineering, Jilin University, 2699 Qianjin Street, Changchun, 130012, China
[c] Department of Mechanical Engineering, University of Minnesota, Minneapolis, MN, 55455, USA

ARTICLE INFO

Article history:
Received 10 January 2018
Received in revised form 3 March 2018
Accepted 23 March 2018
Available online 26 March 2018

Keywords:
NO_2 sensor
CeO_2-B_2O_3 (B = Fe, Cr)
Yttria-stabilized-zirconia
Mixed-potential

ABSTRACT

Mixed-potential type (MPT) NO_2 sensors equipped with CeO_2-B_2O_3 (B = Fe, Cr) sensing electrode (SE) and yttria-stabilized-zirconia (YSZ-8Y) electrolyte are fabricated. The new ceria-based nanocomposites synthesized by sol-gel method improve the NO_2 gas sensing properties significantly. The highest response to NO_2 is found for the sensor using CeO_2-Cr_2O_3 binary oxides with 1:1 Ce/Cr sintered at 800 °C, resulting in 100 mV to 100 ppm with relatively fast response and recovery times at the working temperature of 450 °C. A linear relation is obtained for the sensor with configuration of Pt/YSZ/CeO_2-B_2O_3 (B = Fe, Cr) between potential difference (ΔV) and the logarithm of the concentration of NO_2 from 5 to 200 ppm, which the sensitivities are 40.5 and 74.0 mV/decade, respectively. Additionally, the sensor's reproducibility, selectivity, cross-sensitivity and stability are investigated in details. Furthermore, the mixed potential sensing mechanism and catalytic activity to NO_2 for ceria-based nanocomposites are also discussed.

1. Introduction

With the continuous growth of the retention rate of moto vehicle, the scarcity of resources and environment pollution caused by automobile exhaust emissions have become a challenge to the sustainable development of automobile industry [1,2]. In particular, NO_2 gas exhaust from automobile causing acid rain, photochemical smog and the hole in the ozone layer, which seriously destroyed the ecological environment and endangered the health of human body [3,4]. Therefore, to improve the utilization of fuel and reduce the emission of harmful gases effectively, it is necessary to develop NO_2 sensors in vehicle exhaust systems to accurately measure the concentration of NO_2 gas [5,6]. Because of the advantages of high operation temperature, high humidity tolerance, excellent chemical and mechanical durability, and low cost, yttria-stabilized-zirconia (YSZ) has demonstrated a good application potential for high temperature gas sensors in the vehicle exhaust emission system [7–10].

The mixed-potential-type NO_2 sensor based on 8 mol% Y_2O_3-doped ZrO_2 (YSZ-8Y) and various sensing electrode materials has been fabricated to monitor NO_2 gas. For example, some simple oxide materials including NiO, WO_3, Cr_2O_3 and CuO have been investigated by the early research work [11–20]. Doping of noble metals or oxides in oxide materials can improve the sensing performance and working temperatures. Mirua et al. indicated Au loaded NiO sensing electrode by sputtering process shows better response to NO_2 than pure NiO material [21]. Diao et al. prepared a series of mixed W/Cr oxides sensing materials with different ratios of W and Cr working at 800 °C [22]. Cai et al. used MoO_3 doped In_2O_3 as the sensing electrode which exhibited better NO_2 response compared to pure In_2O_3 at 500 °C [23]. Meanwhile, some complex oxides were discovered and used to detect NO_2 gas. The Perovskite oxide $LaMO_3$ (M = Mn, Fe, Co, Ni) and $SmFeO_3$ were utilized for sensing electrodes of YSZ based NO_2 sensors at mid- temperature of 400–500 °C [24–26]. Mirua and Lu et al. firstly used spinel type oxide to detect NO_2 such as $NiCr_2O_4$, $MnCr_2O_4$ and $CdCr_2O_4$, which indicated high response and sensitivity to NO_2 [27–29].

It has been reported that rare earth oxides can be utilized as promoters to enhance sensing performance of composite material such as catalytic activity, chemical stability, and anti-poison property [30–32]. Especially, CeO_2 has been investigated as an excellent component of the composite oxides such CeO_2-TiO_2, which a great potential for applications to SCR catalysis [33]. Inspired by above

* Corresponding authors.
E-mail addresses: liufangmeng@jlu.edu.cn (F. Liu), tcui@me.umn.edu (T. Cui).

https://doi.org/10.1016/j.snb.2018.03.140
0925-4005/

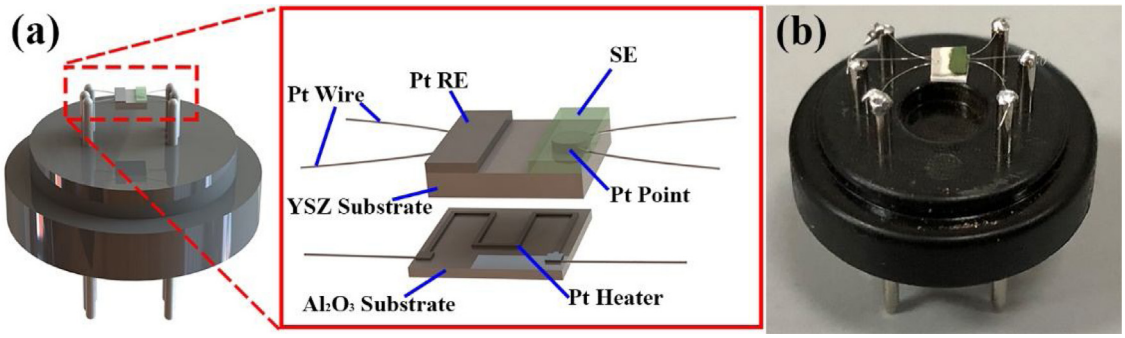

Fig. 1. (a) Schematic diagram of a mixed-potential-type NO_2 sensor based on YSZ electrolyte; (b) The fabricated NO_2 sensor utilizing CeO_2-B_2O_3 (B = Fe, Cr) material.

work, we consider to dope CeO_2 to Fe_2O_3 and Cr_2O_3 for improving the sensing property of simple oxides.

In this paper, a novel CeO_2-B_2O_3 (B = Fe, Cr) binary nanocomposites were synthesized by sol-gel method, and the YSZ based NO_2 sensor with CeO_2-B_2O_3 (B = Fe, Cr) sensing electrode were investigated for the first time. The main purpose of this work is to prove that the high catalytic activity of CeO_2 based binary oxides to NO_2 compared to other type oxides at mid-temperatures. The component and morphology of CeO_2-B_2O_3 (B = Fe, Cr) were characterized completely. Additionally, the sensor's sensing performance was evaluated in details.

2. Experimental

2.1. Materials

The mixed-potential NO_2 sensors were fabricated using a YSZ Chip (8 mol% Y_2O_3-doped, 2 mm × 2 mm × 0.3 mm, Anpeisheng Corp., China) as solid electrolyte. Platinum (Pt) wires 0.01 mm in diameter (Jia Gui Metal Materials Co., Ltd, Shanghai, China) were used to connect electrode and Pt heater to pins. The commercial Platinum (Pt) paste (Sino-platinum Metals Co., Ltd.) used for electrode contacts and a reference electrode. $Ce(NO_3)_3{\cdot}6H_2O$, $Fe(NO_3)_3{\cdot}9H_2O$, $Cr(NO_3)_3{\cdot}9H_2O$ and $C_6H_8O_7{\cdot}H_2O$ (99% AR, Sinopharm Chemical Reagent Co., Ltd, Beijing, China) powders were purchased and utilized as the precursors for sensing electrodes material.

2.2. Synthesis and characterization of CeO_2-B_2O_3 (B = Fe, Cr) sensing material

The CeO_2-B_2O_3 (B = Fe, Cr) binary nanocomposites were synthesized by a conventional sol-gel method. Briefly, 3 mmol $Ce(NO_3)_3{\cdot}6H_2O$ and 3 mmol $Fe(NO_3)_3{\cdot}9H_2O$ were dissolved in deionized water, respectively. After stirring for 30 min, $Ce(NO_3)_3{\cdot}6H_2O$, $Fe(NO_3)_3{\cdot}9H_2O$, $Cr(NO_3)_3{\cdot}9H_2O$ and Citric acid (CA) were mixed up at molar rations of Ce^{3+}: metals (B^{3+}): CA = 1:1:3. The mixture solutions were placed in a beaker heated in water-bath at 80 °C for 3 h, and then dried at 120 °C for 24 h at vacuum drying oven to obtain xerogel precursors. Further, the precursor gel was sintered at 400 °C for 2 h and 800 °C for 5 h in quartz tubular furnace under N_2 atmosphere, respectively. Finally, the powders were introduced into a muffle furnace and sintered at 800 °C for 2 h with a rate of 2 °C/min. As final production, the dark red (CeO_2-Fe_2O_3) and dark green (CeO_2-Cr_2O_3) binary nanocomposites were obtained.

Powder X-ray diffraction (XRD) (Rigaku wide-angle X-ray diffractometer with a monochromator for Cu-Kα radiation at wavelength of 0.1541 nm) was used for analyzing the crystalline structures of synthesized materials. The morphology of the samples was observed by JEOL JSM-6500F field emission scanning electron microscope (FESEM) with an accelerating voltage of 5 kV. The compositions and distributions of various elements with binary nanocomposites were characterized by energy dispersive spectrometer (EDS) mapping. The transmission electron microscope (TEM) image was taken by a JEOL JEM-2100F at 200 kV.

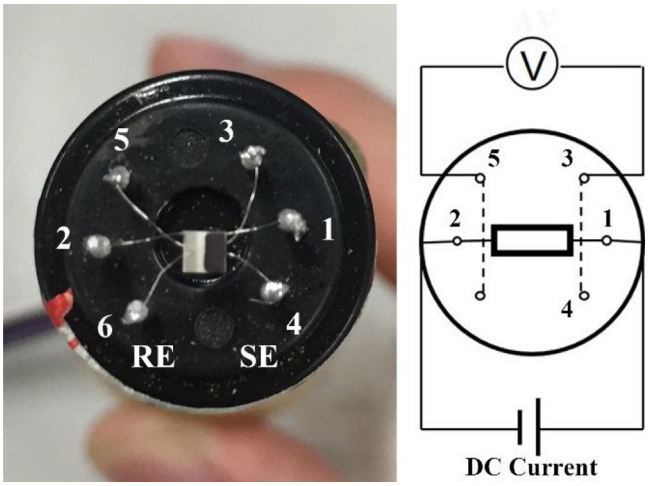

Fig. 2. The design and testing principle of the MTP NO_2 sensor.

2.3. Fabrication and measurement of the sensor

As shown in Fig. 1a, the schematic diagram of the planar NO_2 sensors assembled by YSZ substrates with configuration of Pt (RE)/YSZ/CeO_2-B_2O_3 (B = Fe, Cr) (SE). The reference electrode (RE) was formed by commercial Pt paste. The binary nanocomposite powders were mixed with deionized water, and milling was utilized to fabricate sensing electrodes (SE). The micro heater formed by Pt wires printed on an Al_2O_3 substrate, attached to the back of YSZ substrate by inorganic adhesive, was used to provide the working temperature for NO_2 sensor. The RE and SE were sintered at 1000 °C for 30 min and 800 °C for 2 h, respectively. The fabricated Pt/YSZ/CeO_2-B_2O_3 (B = Fe, Cr) sensor was shown in Fig. 1b.

The gas sensing performance of Pt/YSZ/CeO_2-B_2O_3 (B = Fe, Cr) sensors was measured by a typical static method [34]. The sensor was fixed on the socket and placed in fluid tight chamber 1 (1L) filled with pure air. The certain concentration of test gas was injected to chamber 2 and distributed uniformly. As shown in Fig. 2, the sensor's pins contact the socket firmly. Interface 1–2 were used to provide heating current by a DC power supply (GPD-33038, GWINSTEK), and the electric potential difference (ΔV) between Interface 3–4 (SE) and Interface 5–6 (RE) were measured with a digital electrometer (DM3054, RIGOL). Finally, the response signals of sensor exposed to air (chamber 1) and different concentrations of sample gases (chamber 2) were recorded by the software of the

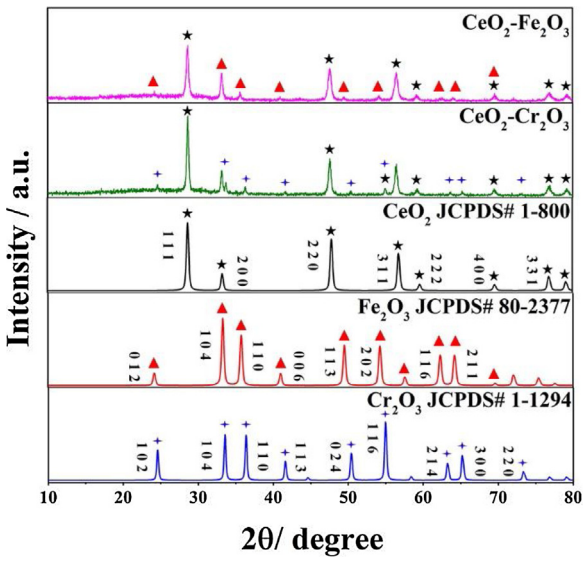

Fig. 3. XRD patterns of CeO_2-Fe_2O_3 and CeO_2-Cr_2O_3 sensing electrode materials.

electrometer. In order to accurately and efficiently achieved the response value during the gas sensing measurement, the response time of the device tested in different concentrations of target gases and air were conformity set as 4 min. Furthermore, the response and recovery values obtained at last second in different gases were used as the potential values for the calibration. The polarization curves and impedance curves of sensors were carried out by dynamic polarization scanner (CHI600C, Instrument Corporation of Shanghai, China) and impedance/gain-phase analyzer (SI 1260, solartron, UK) in the base gas (air) and the different concentration of NO_2 gas at working temperatures.

3. Results and discussion

3.1. Crystal structure and morphology

Fig. 3 presents the XRD patterns of Ce/B (B = Fe, Cr) binary composites. The graphs are plotted between intensity and 2θ, for general conditions 2θ value ranges from 10° to 80°. All peaks could be index to the typical CeO_2 composed with Fe_2O_3 and Cr_2O_3 structures (JCPDS#1-800, JCPDS#80-2377 and JCPDS#1-1294). Additionally, no peaks of other impurities are observed, indicating the successful synthesis of homogenous phase CeO_2-B_2O_3 (B = Fe, Cr) binary oxides by sol-gel method. The sharp and narrow peaks also suggest the high crystallization of composites oxides materials. The corresponding characteristic XRD datas of crystal phase are also summarized in Fig. 3.

The surface profiles of CeO_2-Fe_2O_3 and CeO_2-Cr_2O_3 SEs calcinated at 800 °C were characterized by FESEM, as shown in Fig. 4. The SEM images of Fig. 4a and b reveals the loose structure and mesopore of CeO_2-Fe_2O_3 and CeO_2-Cr_2O_3 sensing electrodes, respectively. Meanwhile, from the high magnification image, the Fe_2O_3 and Cr_2O_3 nanoparticles were tightly bonded with CeO_2 nanoparticles, forming the nanocomposites oxides evidently. Furthermore, Fig. 4(a1–4) and (b1–4) exhibits EDS mapping images of CeO_2-Fe_2O_3 and CeO_2-Cr_2O_3 binary oxides with the component proportion of Ce and B (B = Fe, Cr) is 1:1. The co-existences and dis-

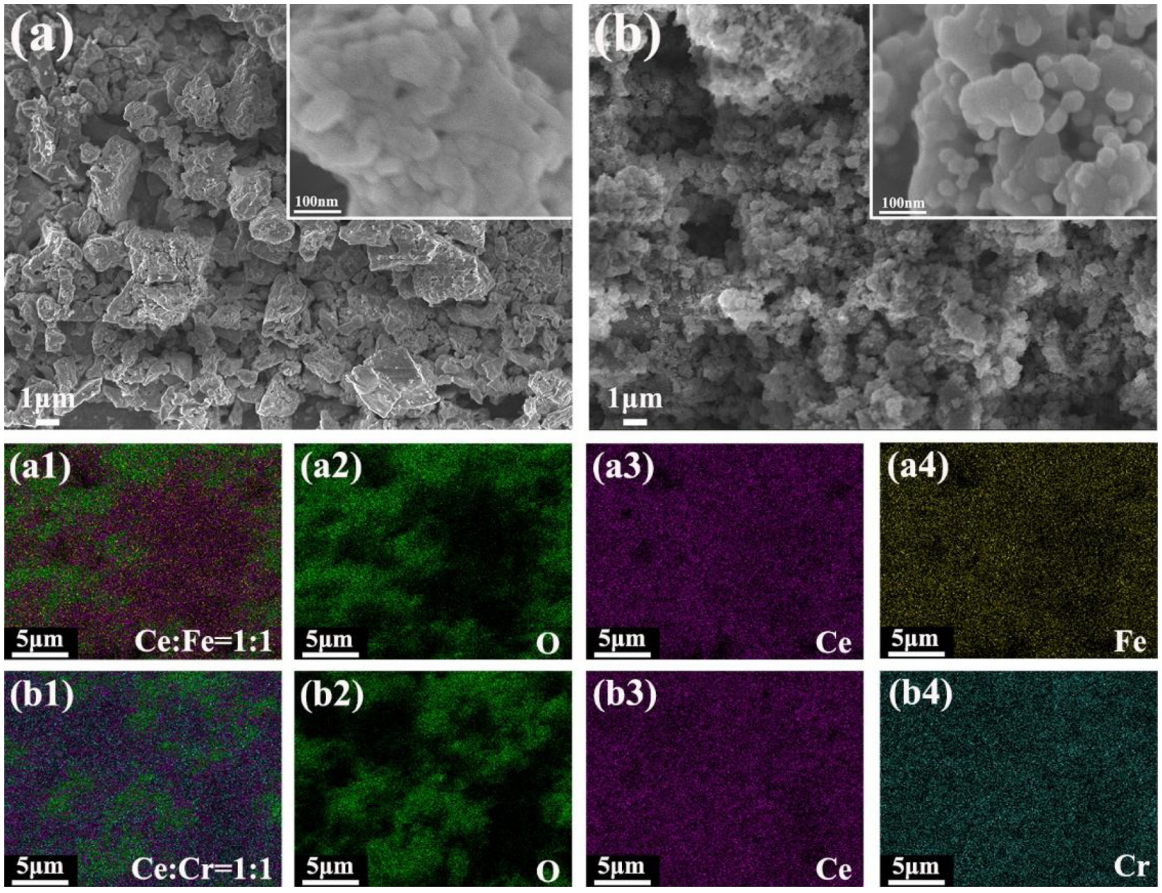

Fig. 4. SEM images of (a) CeO_2-Fe_2O_3 and (b) CeO_2-Cr_2O_3 sensing electrodes; EDS mapping images of (a1-4) CeO_2-Fe_2O_3 and (b1-4) CeO_2-Cr_2O_3 with elements of O, Ce, Fe and Cr.

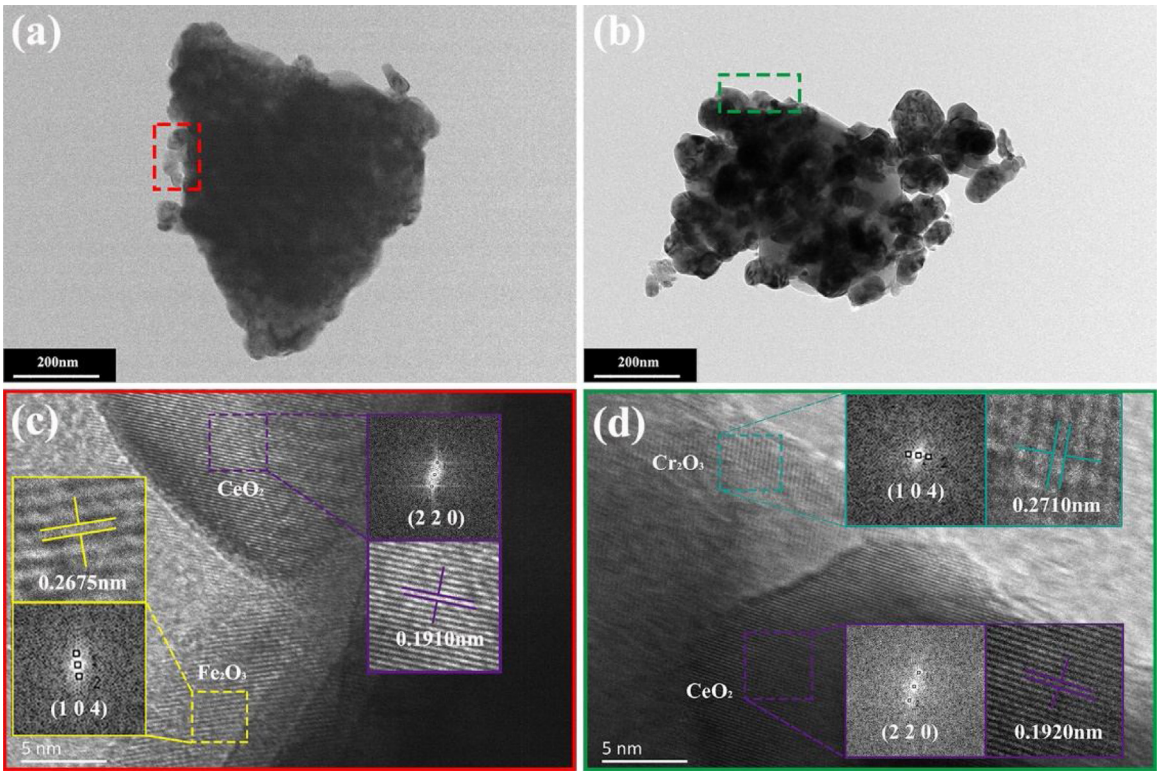

Fig. 5. (a-b) TEM and (c-d) HRTEM images of CeO_2-B_2O_3 (B=Fe, Cr) binary nanocomposites with the planes of Ce (2 2 0), Fe (1 0 4) and Cr (1 0 4).

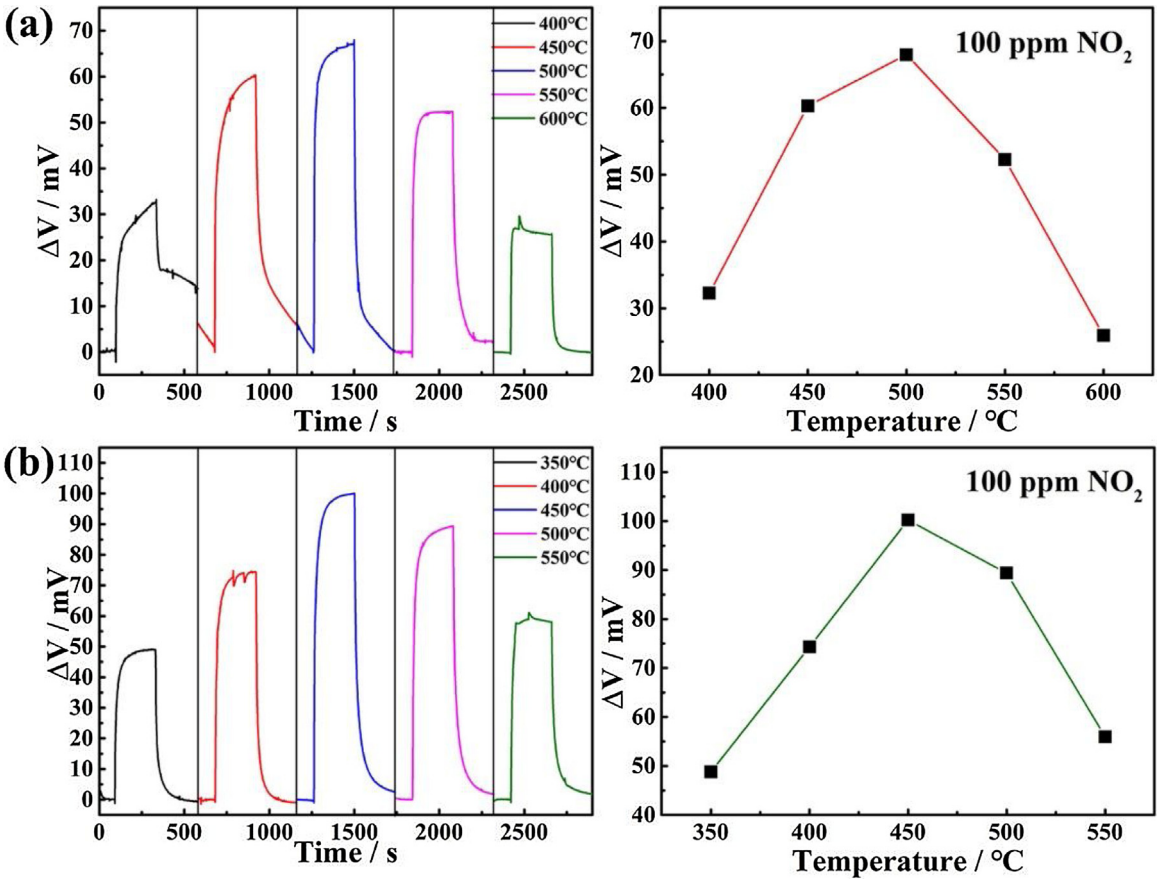

Fig. 6. Response and corresponding values of the NO_2 sensors fabricated by (a) CeO_2-Fe_2O_3 and (b) CeO_2-Cr_2O_3 sensing electrodes to 100 ppm at different operating temperatures.

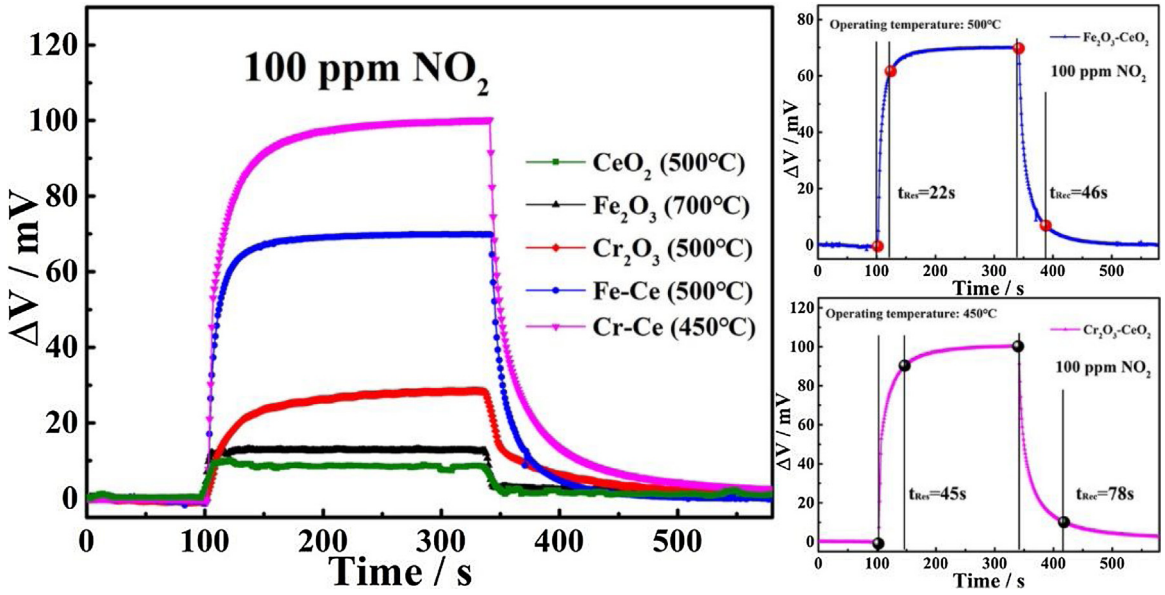

Fig. 7. Response and recovery transients to 100 ppm NO_2 for the sensors based on CeO_2, Fe_2O_3, Cr_2O_3, CeO_2-Fe_2O_3 and CeO_2-Cr_2O_3 sensing electrodes at optimal operating temperatures, respectively.

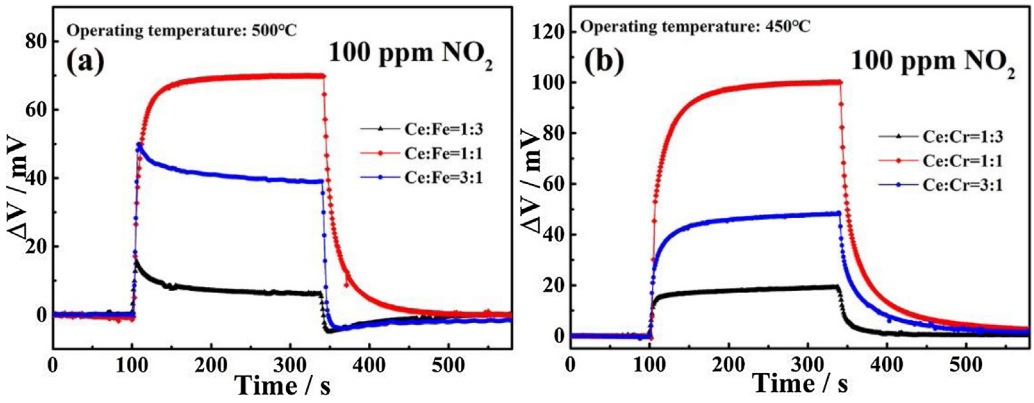

Fig. 8. Response transients of the sensors developed by (a) Ce/Fe and (b) Ce/Cr binary composites with different ratios of Ce and B (B = Fe, Cr) (1:3, 1:1 and 3:1) to 100 ppm NO_2.

tributions of Ce, Fe, Cr and O elements of the CeO_2-B_2O_3 (B = Fe, Cr) binary nanocomposites were confirmed by elemental mapping measurement and calculated precisely. TEM images confirm the crystallinity and particle size of the CeO_2-Fe_2O_3 and CeO_2-Cr_2O_3 binary nanocomposites, as shown in Fig. 5a–b. The edges of the crystals were selected to analyze the crystallite sizes of oxides. As indicated in Fig. 5.c–d, the lattice fringes of the crystals with width of 0.1910 nm, 0.2675 nm and 0.2710 nm observed in HR-TEM, which correspond to the planes of (2 2 0) CeO_2, (1 0 4) Fe_2O_3 and (1 0 4) Cr_2O_3, respectively. This result is in good agreement with that obtained by XRD analysis in Fig. 3.

3.2. Gas sensing properties

As reported in our previous work, the sensing property of the YSZ based gas sensor was highly dependent on the operating temperatures. Thus, the most suitable operating temperatures of the NO_2 sensors fabricated by CeO_2-Fe_2O_3 and CeO_2-Cr_2O_3 sensing electrode were investigated, respectively. The response properties of NO_2 sensors based on CeO_2-Fe_2O_3 and CeO_2-Cr_2O_3 sensing electrodes at different range of working temperatures are demonstrated in Fig. 6. The maximum response value of CeO_2-Fe_2O_3 and CeO_2-Cr_2O_3 sensing material to 100 ppm NO_2 were obtained at 500 °C and 450 °C, respectively. This phenomenon can be explained as the ionic conductivity of YSZ electrolyte is determined by the operating temperatures following the Arrhenius equation [35,36]. Hence, the activation of material is not enough to absolutely support electrochemical reaction at a low operating temperatures, leading to a low response of NO_2. With the increase of operating temperatures, the electrochemical reactivity of the YSZ device was enhanced, and higher response value was achieved. However, the response value decreased due to the desorption of NO_2 on sensing electrodes when the temperature increases further. Consequently, the temperatures at 500 °C and 450 °C were considered to the best operating temperatures of CeO_2-Fe_2O_3 and CeO_2-Cr_2O_3 sensing materials, and used to the subsequent measurement of gas sensing properties.

As a comparison, the sensor's response to NO_2 based on simple oxides (CeO_2, Fe_2O_3 and Cr_2O_3) sensing materials are also discussed. Fig. 7 demonstrates the response and recovery transients of the NO_2 sensors fabricated by CeO_2, Fe_2O_3, Cr_2O_3, CeO_2-Fe_2O_3 and CeO_2-Cr_2O_3 sensing electrodes to 100 ppm NO_2 at optimal operating temperatures, respectively. The sensors based on CeO_2, Fe_2O_3 and Cr_2O_3 exhibits a particularly low electric potential difference (ΔV) (8 mV, 12 mV and 28 mV), poor responsibility, and recoverability. Comparing with the simple oxide sensing mate-

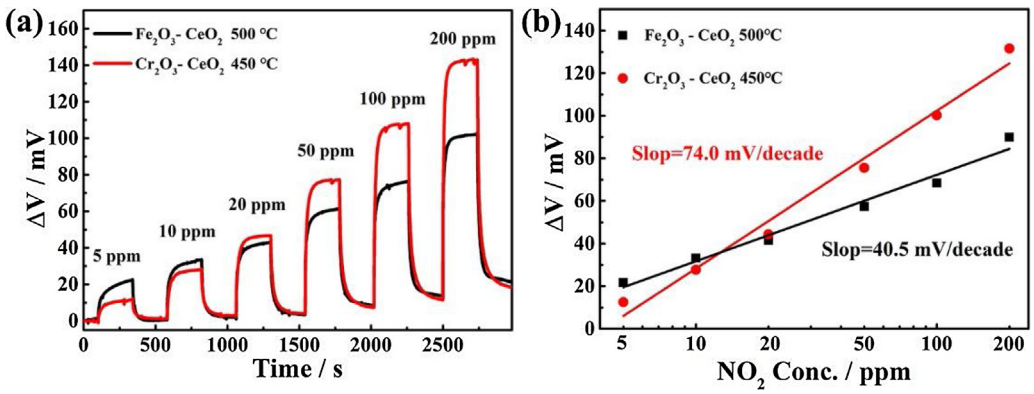

Fig. 9. (a) Response transients of the NO_2 sensors with different sensing electrodes to various NO_2 concentrations in the range of 5–200 ppm at 500 °C and 450 °C; (b) The dependence of the ΔV on the logarithm of NO_2 concentrations for NO_2 sensors.

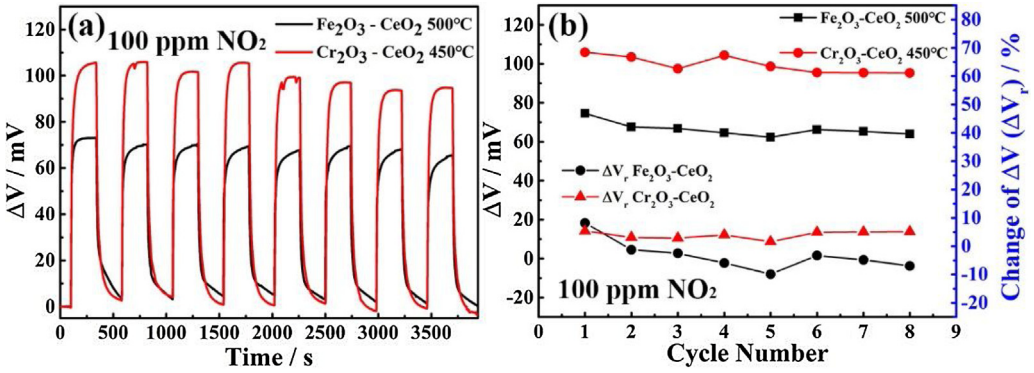

Fig. 10. (a) Continuous response and recovery transients of the NO_2 sensors developed by CeO_2-Fe_2O_3 and CeO_2-Cr_2O_3 sensing electrodes to 100 ppm at 500 °C and 450 °C; (b) Repeat stability of the NO_2 sensors based on different sensing materials to 100 ppm NO_2 for 8 alternative cycles.

rial, the sensors fabricated by CeO_2-Fe_2O_3 and CeO_2-Cr_2O_3 binary nanocomposites demonstrate the relatively fast response (22 and 45 s) and high ΔV value (68 mV and 100 mV) about 5.6 and 3.6 times than simple oxide without CeO_2 to 100 ppm NO_2 correspondingly. Based on above result, the introduction of Ce element oxide has been proved to enhance the response of simple oxide material to NO_2 gas obviously, provided by the superb catalytic activity of CeO_2.

To investigate the influence of the component proportions on the NO_2 sensing properties, the compositions with different ratios of Ce and B (B = Fe, Cr) (1:3, 1:1 and 3:1) were prepared by the sol-gel method, which have been described above. As exhibited in Fig. 8, the response transients of the sensors fabricated by Ce/Fe and Ce/Cr binary oxides with different ratios of Ce and B (B = Fe, Cr) (1:3, 1:1 and 3:1) to 100 ppm NO_2 working at 500 °C and 450 °C. It obviously found that the sensors prepared by Ce/Fe and Ce/Cr sensing electrode with the component proportion of Ce and B (B = Fe, Cr) is 1:1 developed the highest potential difference (ΔV) of 68 mV and 100 mV, which are evidently higher than those for the device with the ratios of 1:3 and 3:1, respectively. Due to the sensors fabricated by Ce/Fe and Ce/Cr sensing electrode with the 1:1 Ce/B (B = Fe, Cr) demonstrated the best responses to NO_2, which were used in subsequent performance testing.

The response and recovery transients of NO_2 sensors fabricated by CeO_2-Fe_2O_3 and CeO_2-Cr_2O_3 sensing electrodes tested with a concentration gradient from 5 to 200 ppm at 500 °C and 450 °C are shown in Fig. 9a. The sensors with CeO_2-Fe_2O_3 and CeO_2-Cr_2O_3 both maintained a good response and recovery to NO_2, and CeO_2-Cr_2O_3 show much better response than CeO_2-Fe_2O_3 at the same NO_2 concentration. As indicated in Fig. 9b, the dependences of ΔV on NO_2 concentrations was also investigated. The sensing signals of ΔV is linearly dependent on the logarithm of NO_2 concentration in the range of 5–200 ppm, conforming the mixed-potential mechanism. The sensitivities of sensors were derived as 40.5 mV/decade (CeO_2-Fe_2O_3) and 74.0 mV/decade (CeO_2-Cr_2O_3) from the linear curve slopes, respectively.

The continuous response-recovery properties of the sensors fabricated by CeO_2-Fe_2O_3 and CeO_2-Cr_2O_3 sensing electrodes with 8 alternating cycles of 100 ppm NO_2 are shown in Fig. 10a. Fig. 10b demonstrates the ΔV and ΔV_r ($\Delta Vr = [\Delta Vn - \Delta V_c]/\Delta Vn \times 100\%$, here ΔV_c and ΔV_n represent the ΔV of single test and nth measurement to 100 ppm NO_2) of sensors based on two different electrode materials to 100 ppm NO_2 with each cycle measurement, and the ΔVr are less than 9.9% and 5.4%, respectively. All these results indicate good repeatability of NO_2 sensors working at a mid-temperatures.

According to the mixed-potential sensing model, the ΔV of sensors is affected by the concentration of oxygen [37,38]. Fig. 11 shows the response of sensors to 100 ppm NO_2 with a variation of oxygen concentration from 2% to 21%, respectively. The result gives that the ΔV value of NO_2 sensors were increased by the decrease of oxygen concentration, almost liner to the logarithm of the oxygen concentration with a negative slope. Such a conclusion was coincided with the mixed-potential mechanism, indicating a relatively good oxygen stability of NO_2 sensors.

In addition, the anti-moisture performance of the NO_2 sensor is also very important due to the humidity variation of the vehicle emission system. Hence, the influence of moisture to NO_2 sensors was investigated. As exhibited in Fig. 12a–b, the response of NO_2 sensors based on CeO_2-Fe_2O_3 and CeO_2-Cr_2O_3 electrodes to 100 and 50 ppm NO_2 gas in the relative humidity (RH) range of 20% to 98% was measured at 500 °C and 450 °C, respectively. The ΔV_h ($\Delta Vh = [\Delta Vn - \Delta V0]/\Delta Vn \times 100\%$, here ΔV_0 and ΔV_n denote the

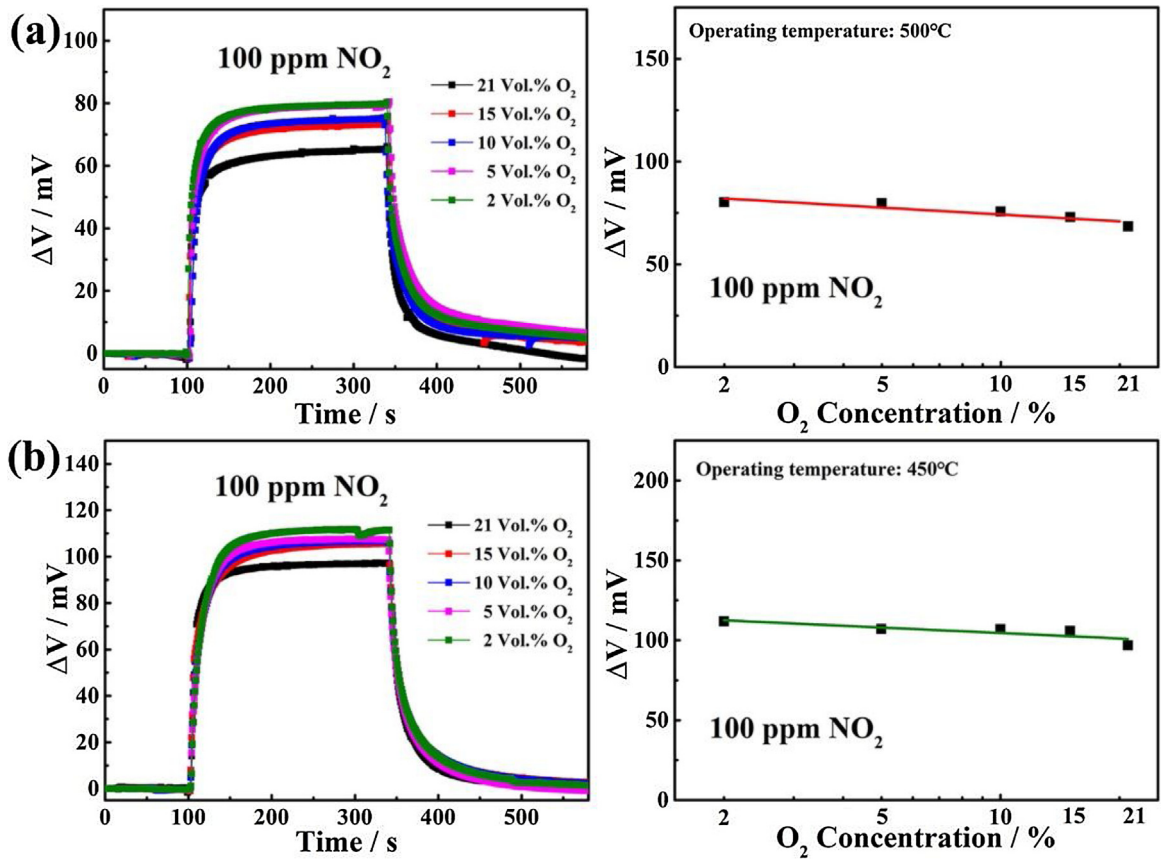

Fig. 11. Responses of the sensors fabricated by (a) CeO_2-Fe_2O_3 and (b) CeO_2-Cr_2O_3 sensing electrodes at different concentrations of O_2 at 500 °C and 450 °C, and the dependence of the ΔV on the logarithm of O_2.

ΔV value of the NO_2 sensor in 10% and n% relative humidity environment to 100 ppm NO_2) was used to explain the change in degree of ΔV with humidity, as shown in Fig. 12c. It can be concluded that the sensor's ΔV changes with the increase of relative humidity. The maximum values of ΔV_h are 15.4% and 19.2% under the condition of relative humidity of 98%, respectively. This phenomenon is almost consistent with the results reported in our previous work. Due to the higher operating temperatures, CeO_2-Fe_2O_3 binary nanocomposites developed a comparatively better moisture resistance and stability than CeO_2-Cr_2O_3 in the high humidity environment.

Considering the complex gas environment of vehicle emission, the selectivity of NO_2 sensor in multiple gases is very important. Selectivity and cross-sensitivity of NO_2 sensors fabricated by CeO_2-B_2O_3 (B = Fe, Cr) sensing electrode to 100 ppm various gases, such as NO, CO, NH_3, CH_4, C_2H_2 and H_2 (0.1%) were measured individually. As indicated in Fig. 13a–b, compared with 100 ppm of NO_2, the response of the sensors to coexistence of NO_2 and other gases slightly changed. This result demonstrates that the sensors with CeO_2-B_2O_3 (B = Fe, Cr) sensing material has a good selectivity and cross-sensitivity to NO_2 gas in the multiple gases atmosphere. Finally, the long-term stability of NO_2 sensors were measured. With small changes in ambient temperature and humidity (20 °C and 10% RH), the NO_2 sensors fabricated by CeO_2-B_2O_3 (B = Fe, Cr) sensing electrode are incessantly working for 20 days at the working temperature of 500 °C and 450 °C, respectively. As shown in Fig. 13c, the sensors developed by two kinds of sensing electrode both maintained good ΔV_s ($\Delta Vs=[\Delta Vs - \Delta V1]/\Delta Vs \times 100\%$, here ΔV_1 and ΔV_s denote the ΔV value of the NO_2 sensor in the 1st and nth day to 100 ppm NO_2) within the little change (less than 9.1% and 5.5%), demonstrating a good long-term stability and reliability.

3.3. Discussion of the sensing mechanism

The principle of the mixed-potential-type sensor is investigated to interpret the enhancement mechanism of the response and sensitivity. The sensor can be described by the electrochemical cells in NO_2 gas as Eq. (1).

$$NO_2 + \text{air}, CeO_2\text{-}B_2O_3(B = Fe, Cr)(RE)/YSZ\text{-}8Y/Pt(RE), NO_2 + \text{air} \quad (1)$$

Apparently, when the sensor is exposed to the NO_2 atmosphere, there are two electrochemical reactions at the triple phase boundary (TPB) of SE as described in Eqs. (2) and (3).

$$\text{Cathode}: NO_2 + 2e^- \rightarrow NO + O^{2-} \quad (2)$$

$$\text{Anode}: 2O^{2-} \rightarrow O_2 + 4e^- \quad (3)$$

$$2NO_2 \rightarrow 2NO + O_2 \quad (4)$$

When the reaction rates of cathode and anode are equal, a local cell was formed, and the potential at SE was called the mixed potential. However, it can be concluded from Eq. (4), the concentration of NO_2 is decreased when arrived at TPB of RE and YSZ. This phenomenon would reduce the amplitude of ΔV and sensitivity of sensors. The response (ΔV) of mixed-potential gas sensors can be explained by Butler-Volmer equation [38,39].

$$E_M = E_0 + mAlnC_{NO_2} - nAlnC_{O_2} \quad (5)$$

As shown in Eq. (5), E_0, m, n and A are constants. When the other factors are fixed (C_{O_2}), the mixed-potential value (E_M) depends on the concentration of NO_2 gas (C_{NO_2}), and utilized as the sens-

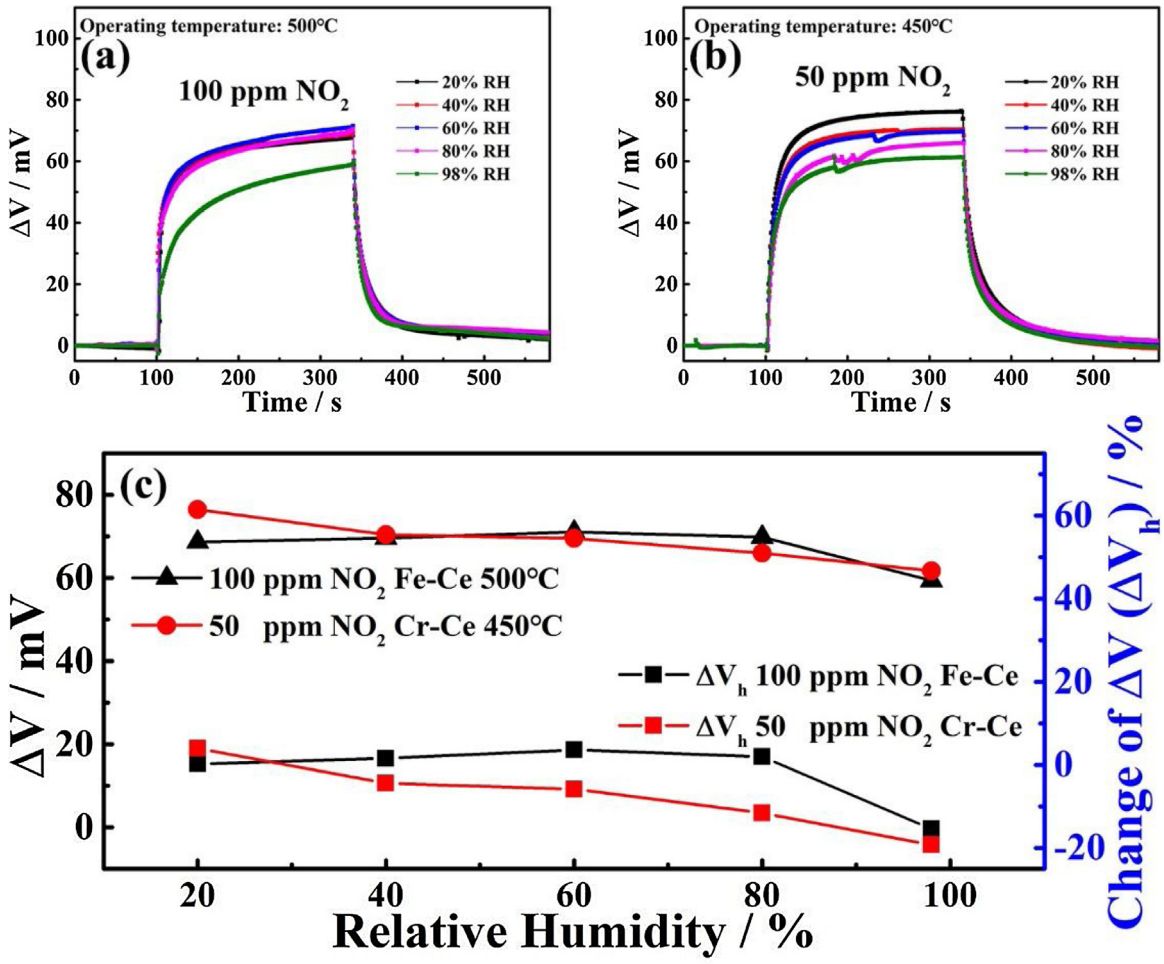

Fig. 12. Responses and recovery transients of the NO_2 sensors attached with (a) CeO_2-Fe_2O_3 and (b) CeO_2-Cr_2O_3 sensing electrodes to 100 and 50 ppm under different relative humidity; (c) Moisture resistance of sensors with different sensing materials to 100 and 50 ppm NO_2 working at 500 °C and 450 °C.

Table 1
The calculating results of N_2 adsorption-desorption experiment to Fe_2O_3-CeO_2 and Cr_2O_3-CeO_2 sensing electrode materials.

Sample	BET surface area (m^2g^{-1})	Pore Volume (cm^3g^{-1})	Average pore size (nm)
Fe_2O_3-CeO_2	2.8509	0.009172	16.0821
Cr_2O_3-CeO_2	11.4732	0.088068	33.7942

Table 2
Comparison of the sensing properties of the mixed-potential type NO_2 sensors with different sensing electrode materials reported in recent literature.

Sensing electrode	Operating temperature (°C)	NO_2 Conc. (ppm)	Response and recovery times (s)	Response value (mV)	Sensitivity (slope) (mV/decade)	Low detection limit (ppm)	Ref.
Fe_2O_3-CeO_2	500	100	30/89	68	40.5	5	This work
Cr_2O_3-CeO_2	450	100	43/84	100	74.0	5	This work
NiO	850	400	20/180	75	–	10	[42]
CuO	700	100	40/100	45	–	100	[19]
NiO-Au	600	400	-/-	73	–	50	[21]
NiO-CuO	800	400	-/-	28	–		[43]
Cr_2O_3-WO_3	800	100	20/-	51.6	25	2	[22]
MoO_3-In_2O_3	500	200	-/-	95	59	10	[23]
$SmFeO_3$	500	90	156/157	64	–	30	[26]
$LaFeO_3$	550	60	-/-	45	–	15	[24]
$(La_{0.8}Sr_{0.2})2FeMnO_{6-\delta}$	600	200	30/115	43.9	62.5	100	[44]
$CdCr_2O_4$	500	200	-/-	65	40	20	[29]
$MnCr_2O_4$	650	100	-/-	73	44.5	5	[28]
$NiCr_2O_4$	550	200	120/-	80	–	25	[27]
$ZnFe_2O_4$	700	200	360/-	41	24	50	[45]

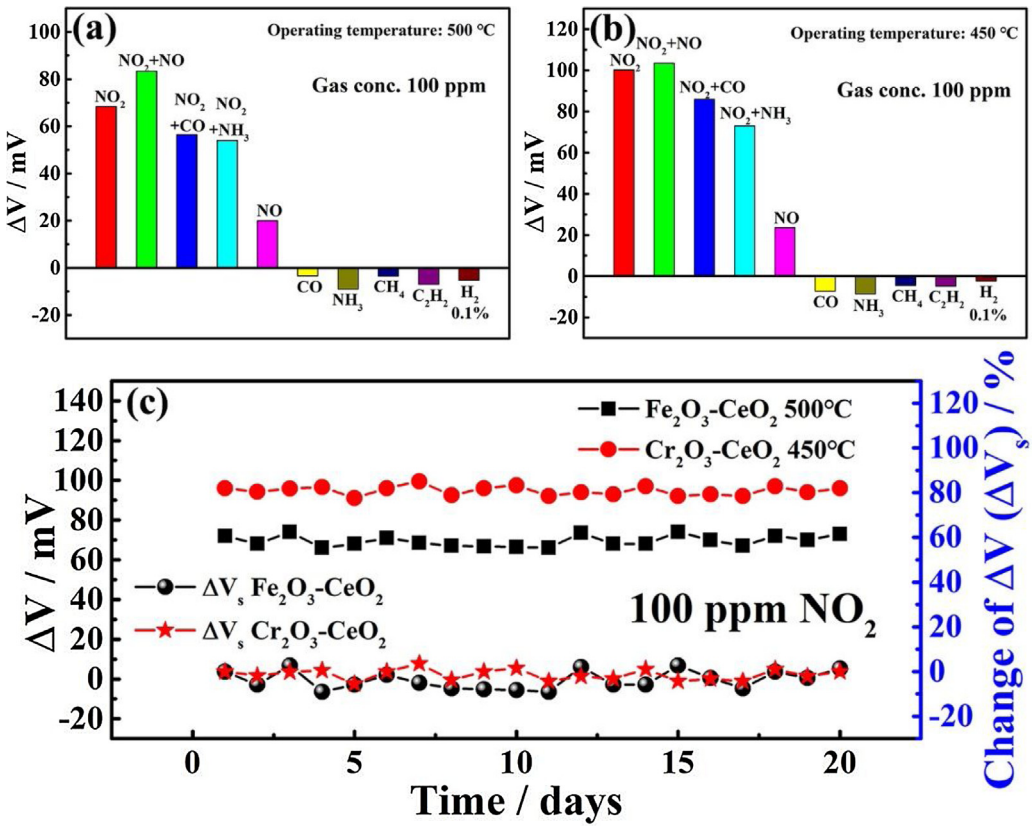

Fig. 13. Cross sensitivities and selectivities to 100 ppm various gases for the sensors fabricated by (a) CeO_2-Fe_2O_3 and (b) CeO_2-Cr_2O_3 sensing electrodes at 500 °C and 450 °C; (c) Long-term stability of the sensor to 100 ppm NO_2 for 20 days.

ing signal of the sensor. In order to explain the enhancement of the response and sensitivity, the component and microstructure of sensing electrode material were considered. Because of the activity of the 4f electron layer, the rare earth materials are usually in the form of oxides, and there are many free oxidation valence states, which can easily gain and lose electrons in the process of oxidation and reduction, thus affecting the reaction properties. Especially, CeO_2 has been investigated as an excellent oxygen storage and supplier due to the free transition between Ce^{4+} and Ce^{3+}, during which procedure dissociated oxygen can be released [40]. The free oxygen released near the compound oxide reactive sites, participating the redox procedure and enhancing the synergistic effect with oxide materials [30,41]. Meanwhile, the oxygen-enriched environment oxidizes NO to NO_2, decreasing the signal attenuation caused by the decomposition of NO_2. This result also explains why the sensor response to the reduction gas of NO is positive, as shown in Fig. 13a–b. Furthermore, the surface area, pore volume and pore size of CeO_2-Fe_2O_3 and CeO_2-Cr_2O_3 binary nanocomposites were measured by Brunauer-Emmett-Teller (BET) method, as listed in Table 1. CeO_2-Cr_2O_3 shows a higher response than CeO_2-Fe_2O_3 material due to the larger surface area and pore volume structure. It provides sufficient reactive sites for redox reaction, and the NO_2 gas can pass through the SE to TPB rapidly and effectively, which avoided the attenuation of mixed-potential value caused by Eq. (4). Table 2 represents the summary of the mixed-potential type YSZ-based NO_2 sensors reported in literature the in recent years. The NO_2 sensors using CeO_2-Fe_2O_3 and CeO_2-Cr_2O_3 as sensing materials exhibit good sensing performance to NO_2 comparatively.

For testifying the sensing mechanism, the polarization curves of sensors based on CeO_2-Fe_2O_3 and CeO_2-Cr_2O_3 electrodes to 20, 50 and 200 ppm NO_2 (with air) were tested, as given in Fig. 14a–b, respectively. Compared with the polarization curve of NO_2 based on CeO_2-Fe_2O_3 sensing electrode to NO_2 with air, the polarization curve of NO_2 based on CeO_2-Cr_2O_3 sensing electrode tends to shift upward obviously. The shift of the polarization curve explains a more intense reaction at cathode Eq. (1), representing the promotion of response. Furthermore, the modified cathodic polarization curves of NO_2 sensors with different electrode materials were measured, as shown in Fig. 14c–d. The anodic curve was measured in pure air, and cathodic curve was obtained by the curve of mixed gas (NO_2 + O_2) subtracts that in air. The theoretical mixed-potential value was obtained by the intersection of the cathodic and anodic curves. As shown in Table 3, the correctness of the mixed-potential mechanism was verified by the calculated potential value and the actually measured value at the same concentration of NO_2 gas.

In order to study the electrochemical reaction of the device, the complex impedance of the devices with CeO_2-Fe_2O_3 and CeO_2-Cr_2O_3 sensing electrodes were tested, respectively. As demonstrated in Fig. 15, the complex impedance spectra of NO_2

Table 3
Corresponding relation of the estimated and observed potential values for the NO_2 sensors fabricated by Fe_2O_3-CeO_2 and Cr_2O_3-CeO_2 sensing electrodes response to different concentrations of NO_2.

Sensing electrode	NO_2 Concentration (ppm)	Mixed potential (estimated) (mV)	Potential difference (ΔV) (observed) (mV)
Fe_2O_3-CeO_2	20	44	41
	50	60	57
	100	66	68
	200	92	90
Cr_2O_3-CeO_2	20	46	44
	50	70	74
	100	99	100
	200	132	132

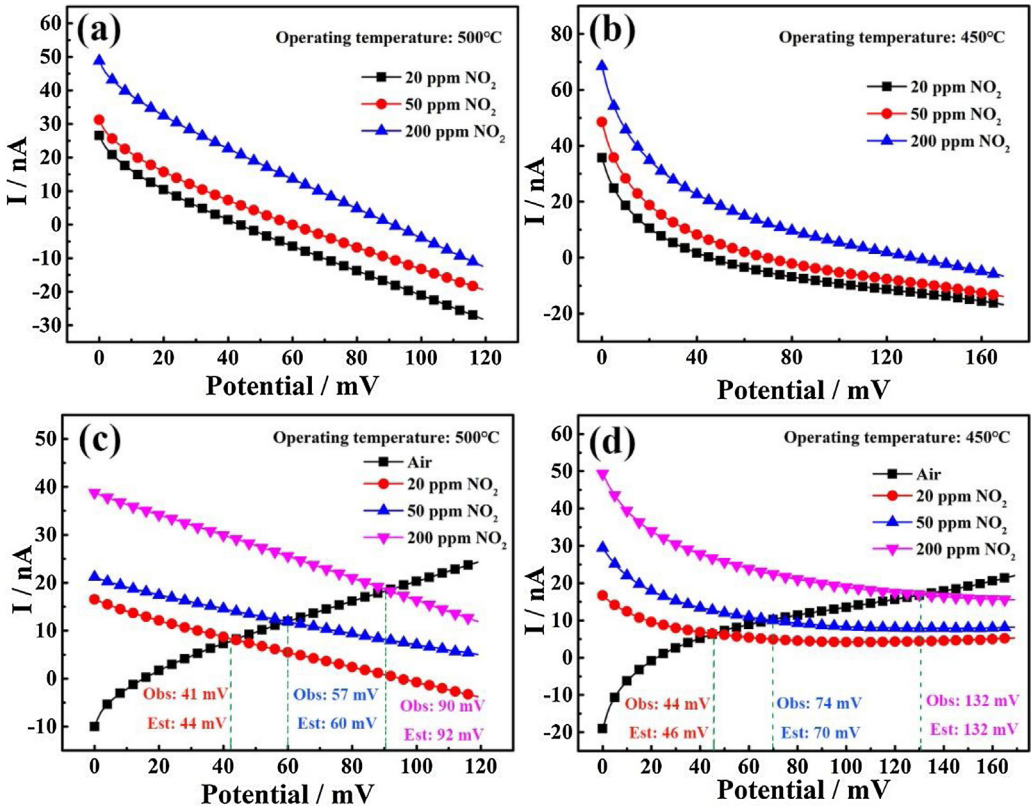

Fig. 14. Polarization curves of the NO_2 sensors attached with (a) CeO_2-Fe_2O_3 and (b) CeO_2-Cr_2O_3 sensing electrodes in 20, 50 and 200 ppm NO_2 (+air); (c-d) The modified polarization curves of the NO_2 sensors to air, 20, 50 and 200 ppm NO_2 at 500 °C and 450 °C.

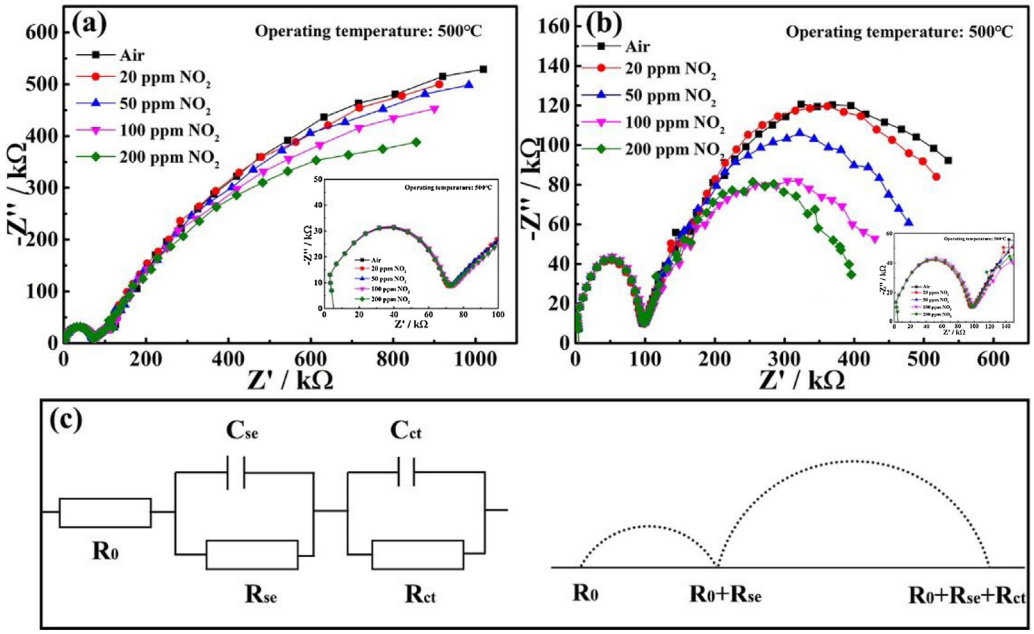

Fig. 15. Complex impedance spectras of the NO_2 sensors based on (a) CeO_2-Fe_2O_3 and (b) CeO_2-Cr_2O_3 sensing electrodes in air, 20, 50, 100 and 200 ppm NO_2 at 500 °C and 450 °C; (c) The equivalent circuit models of NO_2 sensor based on YSZ solid electrolyte.

sensor measured in mixed gas ($NO_2 + O_2$) was described as two semicircular arcs. According to the equivalent circuit model of NO_2 sensor based on YSZ solid electrolyte, as described in Fig. 15c, R_0 is the sum of impedance with the connecting conductor and solid electrolyte, R_{sc} and C_{sc} represents the impedance and capacitance of the sensing electrode, respectively. As shown in Fig. 15a–b, the high frequency semicircle (inset) is related to solid electrolytes and sensing electrode materials, almost unaffected by the concentrations of NO_2 and O_2. R_{ct} denotes the interfacial impedance during the reaction at sensing electrode, where C_{ct} is the double-layer capacitance of the interface of the TPB. The low frequency spectrum (right side) is related to the reaction degree of electrochemical reaction. R_{ct} reflects the intensity of the interfacial electrochemical reaction, indicating the smaller R_{ct} obtained the more intense

of interface reaction occurred. When the device was measured to NO_2, the R_{ct} of NO_2 sensor was evidently decreased by the increase of the concentration of NO_2. Based on the above conclusion, the catalytic activity to electrochemical reaction at TPB was enhanced by the higher concentration of NO_2, consistent with the response tendency to previous measurements.

4. Conclusion

In this work, the high performance YSZ-based mixed-potential type NO_2 gas sensors based on new CeO_2-B_2O_3 (B = Fe, Cr) binary nanocomposites sensing electrode is reported. The NO_2 sensors utilizing CeO_2-Fe_2O_3 and CeO_2-Cr_2O_3 materials with 1:1 Ce/B (B = Fe, Cr) demonstrate fast response, good sensitivity and repeatability to NO_2 concentrations in the range of 5–200 ppm at 500 °C and 450 °C, respectively. Especially, the sensor using the CeO_2-Cr_2O_3 sensing electrode represents the excellent sensitivity of 74.0 mV/decade at 450 °C. Meanwhile, the NO_2 sensors with two different sensing materials display fast response (22 and 46 s) and recovery times (45 and 78 s), good selectivity and long-term stability. In addition, the device with CeO_2-Fe_2O_3 material shows a better anti-moisture performance than CeO_2-Cr_2O_3 with smaller drifts under different relative humidity. These conclusions indicate that ceria-based nanocomposites oxide is a promising sensing material of mixed-potential type NO_2 sensors working at mild temperatures, which maybe lead wide applications to automobile industry.

Acknowledgements

This work was primarily supported by the Open Fund of the State Key Laboratory on Integrated Optoelectronics (Grant NO. IOSKL2017KF09) and the State Key Laboratory of Precision Measurement Technology and Instruments, Tsinghua University. The authors also thank the State Key Laboratory on Integrated Optoelectronics, Jilin University, for their fabrication and measurement service.

References

[1] M.V. Twigg, Progress and future challenges in controlling automotive exhaust gas emissions, Appl. Catal. B: Environ. 70 (2007) 2–15.
[2] R. Moos, B. Reetmeyer, A. Hürland, C. Plog, Sensor for directly determining the exhaust gas recirculation rate—EGR sensor, Sens. Actuators, B 119 (2006) 57–63.
[3] W. Yang, S.T. Omaye, Air pollutants, oxidative stress and human health, Mutat. Res. 674 (2009) 45–54.
[4] M. Fleischer, E. Simon, E. Rumpel, H. Ulmer, Detection of volatile compounds crrelated to human diseases through analysis with chenical sensors, Sens. Actuators, B 83 (2002) 245–249.
[5] N. Miura, M. Nakatou, S. Zhuiykov, Development of NO_x sensing devices based on YSZ and oxide electrode aiming for monitoring car exhausts, Ceram. Int. 30 (2004) 1135–1139.
[6] L.Y. Woo, R.S. Glass, R.F. Novak, J.H. Visser, Diesel engine dynamometer testing of impedancemetric NOx sensors, Sens. Actuators, B 157 (2011) 115–121.
[7] J. Fergus, Materials for high temperature electrochemical NO_x gas sensors, Sens. Actuators, B 121 (2007) 652–663.
[8] K. Mahendraprabhu, P. Elumalai, Stabilized zirconia-based selective NO_2 sensor using sol-gel derived Nb_2O_5 sensing-electrode, Sens. Actuators, B 238 (2017) 105–110.
[9] P.K. Sekhar, E.L. Brosha, R. Mukundan, W. Li, M.A. Nelson, P. Palanisamy, et al., Application of commercial automotive sensor manufacturing methods for NO_x/NH_3 mixed potential sensors for on-board emissions control, Sens. Actuators, B 144 (2010) 112–119.
[10] F. Liu, B. Wang, X. Yang, Y. Guan, R. Sun, Q. Wang, et al., High-temperature stabilized zirconia-based sensors utilizing MNb_2O_6 (M: Co, Ni and Zn) sensing electrodes for detection of NO_2, Sens. Actuators, B 232 (2016) 523–530.
[11] P. Elumalai, N. Miura, Performances of planar NO_2 sensor using stabilized zirconia and NiO sensing electrode at high temperature, Solid State Ionics 176 (2005) 2517–2522.
[12] V. Plashnitsa, T. Ueda, P. Elumalai, N. Miura, NO_2 sensing performances of planar sensor using stabilized zirconia and thin-NiO sensing electrode, Sens. Actuators, B 130 (2008) 231–239.
[13] X. Liang, S. Yang, J. Li, H. Zhang, Q. Diao, W. Zhao, et al., Mixed-potential-type zirconia-based NO_2 sensor with high-performance three-phase boundary, Sens. Actuators, B 158 (2011) 1–8.
[14] S.P. Mondal, P.K. Dutta, G.W. Hunter, B.J. Ward, D. Laskowski, R.A. Dweik, Development of high sensitivity potentiometric NO_x sensor and its application to breath analysis, Sens. Actuators, B 158 (2011) 292–298.
[15] C. López-Gándara, J.M. Fernández-Sanjuán, F.M. Ramos, A. Cirera, Role of nanostructured WO_3 in ion-conducting sensors for the detection of NO_x in exhaust gases from lean combustion engines, Solid State Ionics 184 (2011) 83–87.
[16] H. Jin, Y. Huang, J. Jian, Sensing mechanism of the zirconia-based highly selective NO sensor by using a plate-like Cr_2O_3 sensing electrode, Sens. Actuators, B 219 (2015) 112–118.
[17] N. Szabo, Correlation of sensing behavior of mixed potential sensors with chemical and electrochemical properties of electrodes, Solid State Ionics 171 (2004) 183–190.
[18] L. Peter Martin, A. Quoc Pham, R.S. Glass, Effect of Cr_2O_3 electrode morphology on the nitric oxide response of a stabilized zirconia sensor, Sens. Actuators, B 96 (2003) 53–60.
[19] J. Park, B.Y. Yoon, C.O. Park, W.-J. Lee, C.B. Lee, Sensing behavior and mechanism of mixed potential NO_x sensors using NiO, NiO (+YSZ) and CuO oxide electrodes, Sens. Actuators, B 135 (2009) 516–523.
[20] N. Miura, T. Sato, S.A. Anggraini, H. Ikeda, S. Zhuiykov, A review of mixed-potential type zirconia-based gas sensors, Ionics 20 (2014) 901–925.
[21] V.V. Plashnitsa, T. Ueda, P. Elumalai, T. Kawaguchi, N. Miura, Zirconia-based planar NO_2 sensor using ultrathin NiO or laminated NiO–Au sensing electrode, Ionics 14 (2007) 15–25.
[22] Q. Diao, C. Yin, Y. Liu, J. Li, X. Gong, X. Liang, et al., Mixed-potential-type NO_2 sensor using stabilized zirconia and Cr_2O_3–WO_3 nanocomposites, Sens. Actuators, B 180 (2013) 90–95.
[23] H. Cai, R. Sun, X. Yang, X. Liang, C. Wang, P. Sun, et al., Mixed-potential type NO x sensor using stabilized zirconia and MoO_3–In_2O_3 nanocomposites, Ceram. Int. 42 (2016) 12503–12507.
[24] N.D. Tho, D.V. Huong, H.T. Giang, P.Q. Ngan, G.H. Thai, D.T.A. Thu, et al., High temperature calcination for analyzing influence of 3d transition metals on gas sensing performance of mixed potential sensor Pt/YSZ/$LaMO_3$ (M = Mn, Fe, Co, Ni), Electrochim. Acta 190 (2016) 215–220.
[25] X. Sun, C. Zhang, T. Feng, D. Jiang, Sensing behavior of mixed potential NO_2 sensors equipped with $LaMO_3$ (M = Fe or Cr) sensing electrodes, Ionics 21 (2014) 1725–1730.
[26] H.T. Giang, H.T. Duy, P.Q. Ngan, G.H. Thai, D.T.A. Thu, D.T. Thu, et al., High sensitivity and selectivity of mixed potential sensor based on Pt/YSZ/$SmFeO_3$ to NO_2 gas, Sens. Actuators, B 183 (2013) 550–555.
[27] S. Zhuiykov, T. Nakano, A. Kunimoto, N. Yamazoe, N. Miura, Potentiometric NO_x sensor based on stabilized zirconia and $NiCr_2O_4$ sensing electrode operating at high temperatures, Sens. Actuators, B 3 (2001) 97–101.
[28] Q. Diao, C. Yin, Y. Guan, X. Liang, S. Wang, Y. Liu, et al., The effects of sintering temperature of $MnCr_2O_4$ nanocomposite on the NO_2 sensing property for YSZ-based potentiometric sensor, Sens. Actuators, B 177 (2013) 397–403.
[29] N. Miura, G. Lu, N. Yamazoe, High-temperature potentiometric/amperometric NO_x sensors combining stabilized zirconia with mixed-metal oxide electrode, Sens. Actuators, B 52 (1998) 168–178.
[30] M.P. Rosynek, Catalytic properties of rare earth oxides, Catal. Rev. 16 (1977) 111–154.
[31] S.B. Hammouda, F. Zhao, Z. Safaei, I. Babu, D.L. Ramasamy, M. Sillanpää, Reactivity of novel Ceria–Perovskite composites CeO_2-$LaMO_3$ (M = Cu, Fe) in the catalytic wet peroxidative oxidation of the new emergent pollutant äBisphenol F': Characterization, kinetic and mechanism studies, Appl. Catal. B: Environ. 218 (2017) 119–136.
[32] A. Bueno Lopez, K. Krishna, M. Makkee, J.A. Moulijn, Active oxygen from CeO_2 and its role in catalysed soot oxidation, Catal. Lett. 99 (2005) 203–205.
[33] Y.E. Jeong, P.A. Kumar, D.T. Huong, H.P. Ha, K.-Y. Lee, In situ-DRIFTS study of Sb–V–CeO_2/TiO_2 catalyst under standard and fast NH_3-SCR conditions, Top. Catal. 60 (2017) 755–762.
[34] F. Liu, B. Wang, X. Yang, Y. Guan, Q. Wang, X. Liang, et al., High-temperature NO_2 gas sensor based on stabilized zirconia and $CoTa_2O_6$ sensing electrode, Sens. Actuators, B 240 (2017) 148–157.
[35] C. Zhang, C.-J. Li, G. Zhang, X.-J. Ning, C.-X. Li, H. Liao, et al., Ionic conductivity and its temperature dependence of atmospheric plasma-sprayed yttria stabilized zirconia electrolyte, Mater. Sci. Eng.: B 137 (2007) 24–30.
[36] J. Gong, Y. Li, Z. Tang, Y. Xie, Z. Zhang, Temperature-dependence of the lattice conductivity of mixed calcia/yttria-stabilized zirconia, Mater. Chem. Phys. 76 (2002) 212–216.
[37] N. Miura, G. Lu, N. Yamazoe, Progress in mixed-potential type devices based on solid electrolyte for sensing redox gases, Solid State Ionics 136-137 (2000) 533–542.
[38] N. Miura, T. Raisen, G. Lu, N. Yamazoe, Highly selective CO sensor using stabilized zirconia and a couple of oxide electrodes, Sens. Actuators, B 47 (1998) 84–91.
[39] L. Geyu, N. Miurra, N. Yamazoe, High-temperature hydrogen sensor based on stabilized zirconia and a metal oxide electrode, Sens. Actuators, B 35-36 (1996) 130–135.
[40] E. Friedrich, F. Stefano, Z. Ling, M. Tiziano, A. Cristina, F. Paolo, et al., Electron localization determines defect formation on ceria substrates, Science 309 (2005) 752–754.

[41] S. Chunwen, L. Hong, C. Liquan, Nanostructured ceria-based materials: synthesis, properties, and applications, Energy Environ. Sci. 5 (2012) 8475–8505.
[42] X. Li, G.M. Kale, Influence of sensing electrode and electrolyte on performance of potentiometric mixed-potential gas sensors, Sens. Actuators, B 123 (2007) 254–261.
[43] V.P. Vladimir, U. Taro, M. Norio, Improbement of NO_2 a sensing performances by an additional second component to the nano-structured NiO sensing electrode of a YSZ-Based mixed-potential-type sensor, Appl. Ceram. Technol. 3 (2006) 127–133.
[44] L. Zhou, Q. Yuan, X. Li, J. Xu, F. Xia, J. Xiao, The effects of sintering temperature of $(La_{0.8}Sr_{0.2})_2FeMnO_{6-\delta}$ on the NO_2 sensing property for YSZ-based potentiometric sensor, Sens. Actuators, B 206 (2015) 311–388.
[45] M. Norio, Z. Serge, O. Takashi, H. Masaharu, Y. Noboru, Mixed potential type sensor using stabilized zirconia and $ZnFe_2O_4$ sensing electrode for NO_x detection at high temperature, Sens. Actuators, B 83 (2002) 222–229.

Biographies

Rui You received his B.S. degree from Department of Opto-Electronic Engineering in 2013, Changchun University of Science and Technology, Changchun, China. He is now a Ph.D. student at the Department of Precision Instrument at Tsinghua University, Beijing, China. Currently his research interests mainly include gas sensor and application of MEMS process.

Tianshuang Wang received his BS degree from the Electronics Science and Engineering department, Jilin University, China in 2015. Presently, he is currently working toward the Ph.D. degree in the Electronics Science and Engineering department, Jilin University. His research interests include the synthesis of semiconducting metal oxides materials and their applications in gas sensors.

Hongyan Yu received the B.S. degree from Department of Software Engineering in 2014, Jiangxi Agricultural University, Nanchang, China. He works at Integrated Microsystems Laboratory in Department of Precision Instrument at Tsinghua University, Beijing, China.

Jing Wang received her B.S. degree in applied chemistry in 2009 and the M.S. degree in polymer chemistry and physics in 2012 from Northeast Forestry University in China. Her current research is solid electrolyte gas sensor.

Geyu Lu received the B.Sci. degree in electronic sciences in 1985 and the M.S. degree in 1988 from Jilin University in China and the Dr. Eng. degree in 1998 from Kyushu University in Japan. Now he is a professor of Jilin University, China. His current research interests include the development of chemical sensors and the application of the function materials.

Fangmeng Liu received his PhD degree in 2017 from College of Electronic Science and Engineering, Jilin University, China. Now he is a lecturer of Jilin University, China. His current research interests include the application of functional materials and development of solid state electrolyte gas sensor and flexible device.

Tianhong Cui is currently a Professor of Mechanical Engineering and an Affiliate Senior Member of the graduate faculty in Department of Electrical and Computer Engineering and Department of Biomedical Engineering at the University of Minnesota. He joined the faculty of the University of Minnesota in 2003. From 1995–2003, he held research or faculty positions at Tsinghua University, University of Minnesota, National Laboratory of Metrology in Japan, and Louisiana Tech University, respectively. He was a visiting professor at IMTEK, University of Freiburg in Germany in 2006, and he is holding a visiting professorship at Tsinghua University. His current research interests include MEMS/NEMS and nanotechnology for medical applications.